THE AMERICAN SOCIETY OF MECHANICAL ENGINEERS
345 E. 47 St., New York, N.Y. 10017

90-GT-254

Heat Transfer Characteristics of Turbulent Flow in a Square Channel with Angled Discrete Ribs

S. C. LAU, R. D. McMILLIN, and J. C. HAN
Turbine Heat Transfer Laboratory
Department of Mechanical Engineering
Texas A&M University
College Station, Texas 77843-3123

ABSTRACT

Experiments have been conducted to study the turbulent heat transfer and friction for fully developed flow of air in a square channel in which two opposite walls are roughened with 90° full ribs, parallel and crossed full ribs with angles-of-attack (α) of 60° and 45°, 90° discrete ribs, and parallel and crossed discrete ribs with α = 60°, 45°, and 30°. The discrete ribs are staggered in alternate rows of three and two ribs. Results are obtained for a rib height-to-channel hydraulic diameter ratio of 0.0625, a rib pitch-to-height ratio of 10, and Reynolds numbers between 10,000 and 80,000. Parallel angled discrete ribs are superior to 90° discrete ribs and parallel angled full ribs, and are recommended for internal cooling passages in gas turbine airfoils. For α = 60° and 45°, parallel discrete ribs have higher ribbed wall heat transfer, lower smooth wall heat transfer, and lower channel pressure drop than parallel full ribs. Parallel 60° discrete ribs have the highest ribbed wall heat transfer and parallel 30° discrete ribs cause the lowest pressure drop. The heat transfer and pressure drops in crossed angled full and discrete rib cases are all lower than those in the corresponding 90° and parallel angled rib cases. Crossed arrays of angled ribs have poor thermal performance and are not recommended.

NOMENCLATURE

a	coefficient in roughness functions
b	exponent in roughness functions
c_p	specific heat of air at average bulk temperature, J/(kg.K)
D	hydraulic diameter of square channel, m
dP/dx	streamwise pressure gradient in fully developed region in channel, $(N/m^2)/m$
e	height of ribs, m
e^+	roughness Reynolds number, equation (8)
f	friction factor for square channel with two opposite ribbed walls and two smooth walls, equation (3)
f_{ss}	friction factor for square channel with four smooth walls
$G(e^+, Pr)$	heat transfer roughness function, equation (6)
$\overline{G}(e^+, Pr)$	average heat transfer roughness function, equation (7)
$\dot{m}$	rate of mass flow of air, kg/sec
p	rib pitch, m
P	local static pressure, N/m^2
$\dot{q}''_r$	net heat flux on ribbed walls, W/m^2
$\dot{q}''_s$	net heat flux on smooth walls, W/m^2
$R(e^+)$	roughness function, equation (5)
Re_D	Reynolds number based on channel hydraulic diameter, equation (4)
$\overline{St}$	average Stanton number, the average of St_r and St_s
St_r	Stanton number for ribbed walls in square channel with two opposite ribbed walls and two smooth walls, equation (1)
St_s	Stanton number for smooth walls in square channel with two opposite ribbed walls and two smooth walls, equation (2)
St_{ss}	Stanton number for square channel with four smooth walls
$\overline{(T_{wr} - T_b)}$	ribbed wall/bulk temperature difference in fully developed region in channel, K
$\overline{(T_{ws} - T_b)}$	smooth wall/bulk temperature difference in fully developed region in channel, K
$\bar{u}$	average air velocity, m/sec
x	streamwise coordinate, m
α	rib angle-of-attack, degrees
μ	dynamic viscosity of air at average bulk temperature, $N.sec/m^2$
ρ	density of air at average bulk temperature, kg/m^3
τ_w	wall shear stress, N/m^2

INTRODUCTION

Rib turbulators on the surfaces of internal shaped flow passages in modern gas turbine blades enhance the

*Presented at the Gas Turbine and Aeroengine Congress and Exposition—June 11-14, 1990—Brussels, Belgium
This paper has been accepted for publication in the Transactions of the ASME
Discussion of it will be accepted at ASME Headquarters until September 30, 1990

heat transfer to the cooling air. Researchers have modeled these rib-roughened cooling passages as straight and/or multipass rectangular channels with two opposite ribbed walls and two smooth walls. Earlier work includes that of Burggraf (1970), who studied turbulent heat transfer and friction for flow in a square duct with 90° full rib arrays (ribs which stretch across the width of the channel with an angle-of-attack, α, of 90°) on two opposite walls and two smooth walls. Han (1984, 1988), Han et al. (1985, 1989), Han and Park (1988), and Han and Zhang (1989) studied the effects of varying the channel aspect ratio (0.25 to 4.0), the rib angle-of-attack (α = 30°, 45°, 60°, and 90°), the rib pitch-to-height ratio (p/e = 10 to 40), and rib height-to-channel hydraulic diameter ratio (e/D = 0.021 to 0.063) on the heat transfer in straight, square and rectangular channels with full ribs on two opposite walls and two smooth walls. For a square channel, although parallel 60° full ribs enhanced the channel heat transfer the most, they also caused the highest pressure drop. Parallel full ribs with α = 45° and 30° had the best thermal performance, that is, the highest cooling rate for a given pumping power. For a rectangular channel, the increase in the ribbed wall heat transfer was higher with parallel angled full ribs on the narrower walls than with parallel angled full ribs on the wider walls, for a given pumping power. In general, parallel angled full ribs enhanced the ribbed wall heat transfer more than crossed angled full ribs.

Lau et al. (1989) conducted experiments to study the effects of replacing the aligned 90° full ribs on two opposite walls of a square channel with discrete ribs (five equal segments of the 90° full ribs staggered in alternate rows of three and two ribs, aligned rows on the opposite walls) on the turbulent heat transfer and friction for fully developed flow of air in the square channel. The rib configurations examined were: full ribs with α = 90°, discrete ribs with α = 90°, parallel and crossed arrays of discrete ribs (ribs on opposite walls were turned in the same direction and in opposite directions with respect to the main flow, respectively) with α = 60°, 45°, and 30°, and parallel arrays of discrete ribs with α = 45° and -45° on alternate rows. The rib height-to-hydraulic diameter ratio and the rib pitch-to-height ratio were 0.0625 and 10, respectively. The Reynolds number ranged from 10,000 to 80,000. Results showed that the average Stanton number in the 90° discrete rib case was about 10 to 15 percent higher than that in the 90° full rib case. Turning the discrete ribs on the opposite walls 60°, 45°, or 30° in the same direction with respect to the main flow increased the average Stanton number 10 to 20 percent over that in the 90° discrete rib case. Parallel angled discrete ribs with α = 60°, 45°, and 30° had comparable performances and had higher overall heat transfer per unit pumping power than 90° discrete ribs. Crossed arrays of angled discrete ribs performed poorly compared with 90° discrete ribs and were not recommended.

In Lau et al. (1989), the angled discrete ribs were equal-length segments of the 90° full ribs (that is, the lengths of the angled discrete ribs and the 90° discrete ribs were the same). They were arranged in the same arrays as the 90° discrete rib arrays but were turned various angles equal to the angles-of-attack with respect to the main flow. The thermal performances of the angled discrete ribs were compared to those of the 90° full ribs and 90° discrete ribs only.

The objectives of this investigation are to study the turbulent heat transfer and friction for fully developed flow in a square channel with angled discrete ribs on two opposite walls and to compare the thermal performances of corresponding angled full ribs and angled discrete ribs. The study examines the effects on the channel heat transfer and friction of cutting the angled full ribs in prior investigations into five equal segments and staggering them in alternate rows of three and two ribs.

This study differs from that in Lau et al. (1989) in that:

(1) the heat transfer and friction characteristics, and thermal performances of corresponding angled discrete ribs and angled full ribs are compared;

(2) the angled discrete ribs in this study are equal-length segments of the corresponding angled full ribs (that is, the total length of the five angled discrete ribs over each pitch is equal to the length of a corresponding angled full rib) and the ribs in each row are collinear (along an oblique line at an angle equal to the angle-of-attack with respect to the main flow);

(3) this study compares the thermal performances of corresponding parallel and crossed angled full ribs in addition to those of corresponding parallel and crossed angled discrete ribs.

Airflow over a staggered array of angled discrete ribs on a wall separates not only at the top edges of the ribs but also at the edges at the ends of the ribs. The secondary flow near the wall resulting from flow separation at the ends of the ribs interrupts the growth of the boundary layers downstream of the nearby reattachment zones. This secondary flow around the ends of the ribs interacts with the secondary flow caused by the orientation of the ribs, and with the separation from the top edges of the ribs and the reattachment on the wall of the main flow. As a result of the vigorous mixing of the flowing air near the wall and the slight increase in the rib surface area, angled discrete ribs are believed to enhance the heat transfer to the airstream more than angled full ribs.

EXPERIMENTAL APPARATUS

The test apparatus (see Fig. 1A) is an open air flow loop that consists of a centrifugal blower, a settling chamber, a flow diverter (to control the air flow rate), a calibrated orifice flow meter, a flow straightener, an entrance section, and the test section. The aluminum test section is a straight, 1.52 m long channel with a square cross section of 7.62 cm by 7.62 cm. The four walls of the channel are heated individually with electric heaters. The heaters on opposite walls are connected in parallel electrically. A 1.59 mm thick asbestos gasket minimizes the heat transfer between adjacent walls.

Full ribs or discrete ribs, which are cut from 4.76 mm by 4.76 mm square brass bars, are attached to the interior surfaces of two opposite channel walls with silicone rubber adhesive. Therefore, the rib height-to-channel hydraulic diameter ratio, e/D, in this study is 0.0625. The interior surfaces of the other two opposite walls are smooth.

Twelve rib configurations are studied: 90° full ribs, parallel and crossed arrays of full ribs with α = 60° and 45°, 90° discrete ribs, and parallel and crossed arrays of discrete ribs with α = 60°, 45°, and 30°. In all twelve cases, the rib pitch-to-height ratio, p/e, is 10; the rows on the opposite walls are

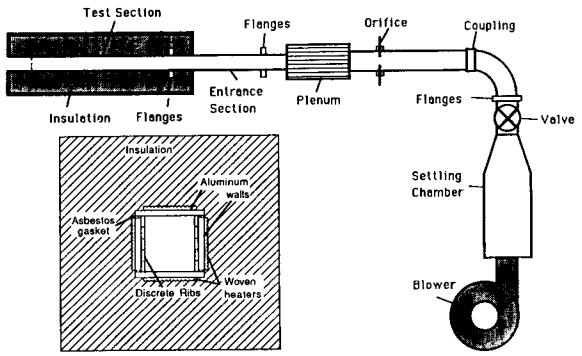

Fig. 1A Schematic of Flow Loop and Test Section Cross Section

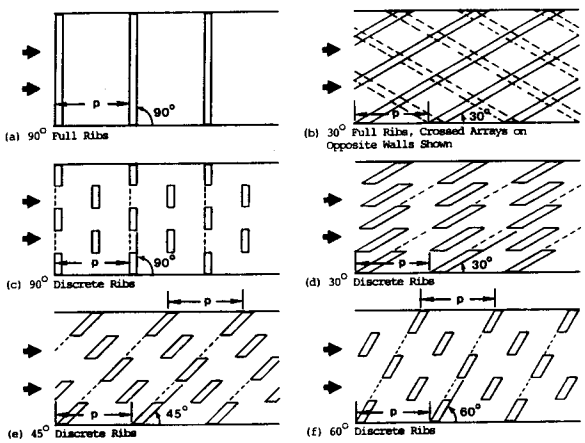

Fig. 1B Typical Rib Configurations

aligned; and the first rows on both walls are at the channel entrance (x = 0). Discrete ribs are staggered on the walls in alternate rows of three and two ribs (see Fig. 1B). Table 1 gives the lengths and orientations of the ribs in the twelve cases. In cases 2a, 3a, 5a, 6a, and 7a, the angled rib arrays on the two opposite walls are parallel (parallel arrays). In cases 2b, 3b, 5b, 6b, and 7b, the angled rib arrays on the two opposite walls are oriented in opposite directions with respect to the main flow (crossed arrays).

Up to 320 ribs are needed in each of the discrete rib cases studied. All of the ribs in each full or discrete rib case are cut individually to precisely the same length (nominal length ± 0.025 mm) with a slitting saw on a milling machine. The angled ribs are cut at an angle equal to the angle-of-attack such that, after the ribs are installed, the end surfaces of the ribs are parallel to the two walls with no ribs. To attach a rib onto a channel wall, a template is used to position the rib accurately. Pressure is applied on the top surface of the rib to squeeze out as much silicone rubber adhesive as possible from under the rib to ensure good metal-to-metal contact between the rib and the channel wall. The thickness of the thin silicone layer is less than 0.01 cm. The thermal resistance between the rib and the channel wall is estimated to be negligible. It takes approximately ten hours to attach all 320 discrete ribs onto the two

TABLE 1. Configurations of Ribs on Channel Walls

Case	Rib Length# (cm)	Rib Configuration, Arrays on Opp. Walls	Rib Angle-Of-Attack
1*	7.62	full	90°
2a	8.80	full, parallel	60°
2b	8.80	full, crossed	60°
3a	10.78	full, parallel	45°
3b	10.78	full, crossed	45°
4*	1.52	discrete	90°
5a	1.76	discrete, parallel	60°
5b	1.76	discrete, crossed	60°
6a	2.16	discrete, parallel	45°
6b	2.16	discrete, crossed	45°
7a	3.05	discrete, parallel	30°
7b	3.05	discrete, crossed	30°

Length of ribs are measured along the rib centerlines
* These results were reported in Lau et al. (1989)

opposite walls of the test channel.

A 1.52 m long acrylic entrance channel provides hydrodynamically fully developed flow at the test section entrance. The test section and the downstream half of the entrance section are heavily insulated with layers of fiberglass felt.

To determine the streamwise wall temperature distributions, forty-two 30-gage copper-constantan thermocouples are installed along the axial centerlines of one of the ribbed walls and each of the smooth walls (at 0.25, 3.25, 6.25, 9.25, 12.25, 15.25, 16.25, 16.75, 17.25, 18.25, 21.25, 24.25, 27.25, and 30.25 times the rib pitch from the channel entrance). Six other thermocouples are installed along two off-center lines at x/p = 16.25, 16.75, and 17.25 on two adjacent walls to check the spanwise variations of the wall temperatures. Each of these axial lines is halfway between the centerline and an adjacent edge of a smooth wall or a ribbed wall. Results show that the variations between the temperatures at these stations along the off-center axial lines and those at corresponding adjacent stations along the axial centerlines are always smaller than the estimated uncertainty of the thermocouple readings (0.28°C). This means that the temperature of the centerline point can represent the spanwise-averaged temperature because of the high thermal conductivity of the aluminum wall.

Each thermocouple is installed in a small hole drilled on the channel wall. The junction of the thermocouple is affixed to the bottom of the hole with silver-based paint and fast drying epoxy. An ohmmeter checks to ensure good physical contact between the thermocouple and the channel wall. Two additional thermocouples measure the inlet air temperature and four thermocouples the exit air temperature. An Omega 410B digital temperature indicator with a 0.1°C resolution reads the thermocouple output.

Three pressure taps are installed along the axial centerline of one of the smooth walls at 0.46 m, 0.91 m, and 1.37 m, respectively, from the test section entrance to determine the streamwise pressure drop. A micromanometer measures the pressures at these taps. Other U-tube and inclined manometers measure the pressure drop across the orifice and the gage pressure

upstream of the orifice.

Two variable transformers control the power input to the four heaters. A Hewlett Packard 3478A multimeter and a Keithley 175 autoranging multimeter measure the voltage drop across each heater and the current through each heater, respectively.

EXPERIMENTAL PROCEDURE

After the ribs are installed and the test section is assembled and checked for air leakage, the blower is switched on to let a predetermined rate of air flow through the flow loop. The test section is then heated to maintain the wall temperatures near the exit at 15°C above the exit air temperature. More power is supplied to the two ribbed wall heaters than to the two smooth wall heaters so that, at any axial location, the wall temperatures on the two ribbed walls and the two smooth walls are about the same.

After steady state is attained in about two hours, all temperatures and pressures are recorded. The maximum variations of some of the readings are also recorded for the uncertainty analysis of the results. The barometric pressure is read at the beginning and the end of a test run.

In separate no-flow experiments, the rate of heat loss through the fiberglass insulation during a test run is determined. By varying the rate of heat input to the heaters and measuring the corresponding average steady state wall temperature, a correlation between the rate of heat input, which is also the rate of heat loss through the fiberglass insulation, and the average wall temperature is obtained. The correlation estimates the rates of heat loss through the insulation at the various wall temperature measurement stations during a test run. For low Reynolds number runs, the total heat loss through the insulation can be up to 7 percent of the total heat input.

DATA REDUCTION

The results of the ribbed wall and smooth wall heat transfer are expressed in dimensionless form as Stanton numbers for the ribbed walls and the smooth walls. They are calculated, respectively, from

$$St_r = \dot{q}''_r D^2/[\dot{m}c_p(\overline{T_{wr}} - T_b)] \quad (1)$$

and

$$St_s = \dot{q}''_s D^2/[\dot{m}c_p(\overline{T_{ws}} - T_b)] \quad (2)$$

In each of the above equations, the rate of net heat input is the measured power input to each heater minus the rate of heat loss through the insulation taking into account the rate of streamwise heat conduction in the channel walls. The heat flux is the rate of net heat input divided by the projected heat transfer area (not including the increased rib surface area). The net heat flux and the average wall/bulk temperature difference are determined over a section of the test channel far downstream of the entrance, where the streamwise wall temperature distribution is linear. The distribution of the bulk temperature is evaluated from energy balance with the rate of net heat transfer from all four walls to the air and the inlet bulk temperature. Since results show that there is no significant difference between the temperature distributions on the two smooth walls even in the parallel angled rib array cases, the smooth wall

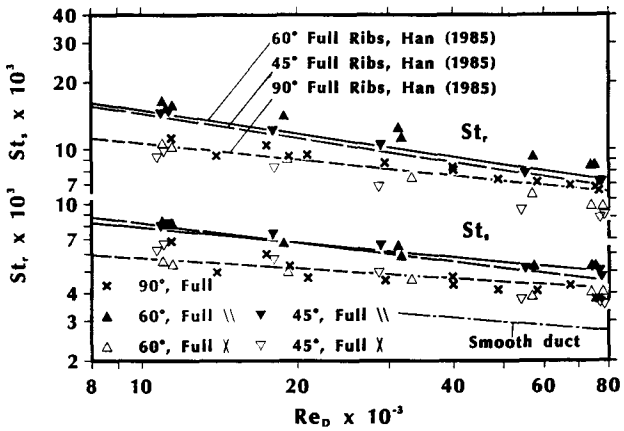

Fig. 2 Ribbed Wall and Smooth Wall Stanton Numbers as Functions of Reynolds Number, Full Rib Cases

Stanton number is presented as the average of the Stanton numbers for the two smooth walls. The average Stanton number, St, is the average of the Stanton numbers for the ribbed walls and the smooth walls.

The friction factor and the Reynolds number are defined respectively as

$$\bar{f} = \tau_w/[(1/2)\rho\bar{u}^2] = [(-dP/dx)D/4]/[(1/2)\rho\bar{u}^2]$$
$$= [(-dP/dx)D^5/[2(\dot{m}^2/\rho)] \quad (3)$$

$$Re_D = \rho\bar{u}D/\mu = \dot{m}/(D\mu) \quad (4)$$

All properties of the flowing air in equations (1) through (4) are evaluated at the average bulk temperature.

The maximum uncertainties of the values of the Reynolds number and the Stanton numbers are estimated to be ±2.9 percent and ±5.8 percent, respectively (Kline and McClintock, 1953). The maximum uncertainty of the values of the friction factor is ±10.9 percent for Reynolds numbers of about 10,000 and ±6.5 percent for Reynolds numbers above 20,000. The large uncertainties of $\bar{f}$ at low Reynolds numbers are the results of the small pressure drops in the test section in the low flow rate cases.

The friction factor and the Stanton numbers are compared to their corresponding values for fully developed turbulent flow through a square channel with four smooth walls, f_{ss} and St_{ss}, which are calculated with the modified Karman-Prandtl and Dittus-Boelter equations (Han, 1984), respectively.

To correlate the data, the roughness function, $R(e^+)$, the heat transfer roughness function, $G(e^+, Pr)$, and the average heat transfer roughness function, $\bar{G}(e^+, Pr)$, are determined with the following equations (Han, 1988).

$$R(e^+) = [(2\bar{f} - f_{ss})/2]^{-0.5} + 2.5\ \ln[2(e/D)] + 2.5 \quad (5)$$

$$G(e^+, Pr) = [(2\bar{f} - f_{ss})/2]^{0.5}/St_r + 2.5\ \ln[2(e/D)] + 2.5 \quad (6)$$

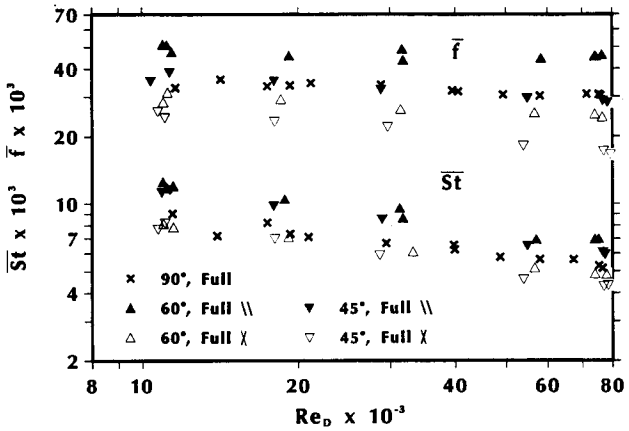

Fig. 3 Average Stanton Number and Friction Factor as Functions of Reynolds Number, Full Rib Cases

$$\bar{G}(e^+, Pr) = [(2\bar{f} - f_{SS})/2]^{0.5}/\overline{St} + 2.5 \ln[2(e/D)] + 2.5 \quad (7)$$

In the above equations, e^+ is the roughness Reynolds number, which is defined as

$$e^+ = (e/D)\, Re_D\, [(2\bar{f} - f_{SS})/2]^{0.5} \quad (8)$$

The roughness functions are correlations for the prediction of the friction factor and Stanton numbers.

PRESENTATION OF RESULTS

This investigation examines how the heat transfer and friction for airflow in a square channel are affected when angled full ribs on two opposite walls of the channel are replaced by angled discrete ribs. Heat transfer, friction, and thermal performance results for the full rib cases are presented first. They are followed by the results for the parallel and crossed discrete rib cases. Lastly, the heat transfer, friction, and thermal performances in corresponding angled full and discrete rib cases are compared and the roughness functions, $R(e^+)$, $G(e^+, Pr)$, and $\bar{G}(e^+, Pr)$, are presented.

Full Rib Arrays

Figures 2 through 4 show the ribbed wall and smooth wall Stanton numbers, the average Stanton number and the friction factor, and the ratios $[(St_r/St_{SS})/(\bar{f}/f_{SS})^{1/3}]$ and $[(\overline{St}/St_{SS})/(\bar{f}/f_{SS})^{1/3}]$ as functions of the Reynolds number in the full rib cases (cases 1, 2a, 2b, 3a, and 3b, with darkened symbols for the parallel rib cases and open symbols for the crossed rib cases), respectively. Clearly, parallel 60° full ribs enhance the ribbed wall heat transfer more than parallel 45° full ribs, which, in turn, cause higher heat transfer on the ribbed walls than 90° full ribs. The smooth wall Stanton numbers in the parallel 60° and 45° full rib cases are comparable and are considerably higher than that in the 90° full rib case.

Parallel 60° full ribs have higher overall heat transfer and pressure drop than parallel 45° full ribs and 90° full ribs. While the average Stanton number in the parallel 45° full rib case is much higher than that

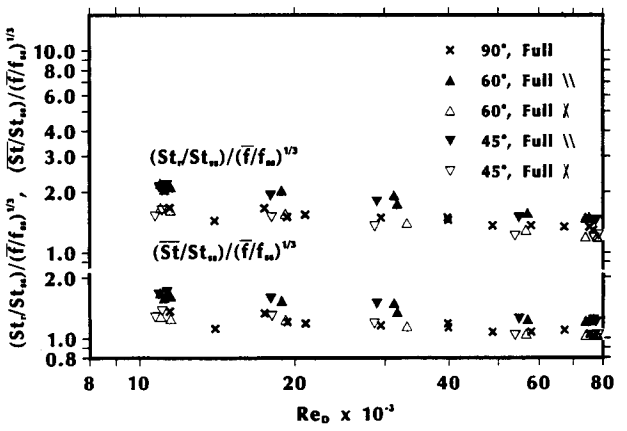

Fig. 4 Thermal Performances of Full Ribs, $[(St_r/St_{SS})/(\bar{f}/f_{SS})^{1/3}]$ and $[(\overline{St}/St_{SS})/(\bar{f}/f_{SS})^{1/3}]$ as Functions of Reynolds Number

in the 90° full rib case, the friction factors in the two cases are comparable —— $\bar{f}$ in case 3a is slightly higher than that in case 1 at low Reynolds numbers and slightly lower than that in case 1 at high Reynolds numbers. The thermal performances of parallel 60° and 45° full ribs are superior to that of 90° full ribs. Han (1985) and Han and Park (1988) reported similar findings.

The present 90° and parallel full rib results are compared to corresponding results from Han (1985) in Fig. 2. The variations between the 90° and parallel 45° full rib results in the two studies are within the estimated experimental uncertainties. However, the ribbed wall Stanton number in the present parallel 60° full rib case is about 15 percent higher than that reported in Han (1985). In this study, all test runs in the parallel 60° full rib case are repeated and the two new sets of data are consistent with each other.

Crossed 60° and 45° full ribs cause lower heat transfer on the ribbed walls, lower overall heat transfer, and lower pressure drop than 90° full ribs. Their thermal performances are only comparable to that of 90° full ribs.

Parallel Discrete Rib Arrays

Parallel angled discrete rib results and 90° discrete rib results are compared in Figs. 5, 6, and 7. Parallel 60° and 45° discrete ribs have higher ribbed wall heat transfer and overall heat transfer than parallel 30° discrete ribs, which, in turn, have higher ribbed wall heat transfer and overall heat transfer than 90° discrete ribs. The ribbed wall Stanton numbers in the parallel 60° and 45° discrete rib cases are about 32 and 18 percent higher than that in the 90° discrete rib case at Re_D = 10,000 and 80,000, respectively. Parallel 60° discrete ribs cause the highest pressure drop while parallel 30° discrete ribs cause the lowest pressure drop. As a result, parallel 45° and 30° discrete ribs outperform parallel 60° discrete ribs in enhancing the heat transfer to the cooling air per unit pumping power.

Crossed Discrete Rib Arrays

Figures 8, 9, and 10 show that the ribbed wall Stanton numbers, the smooth wall Stanton numbers, the average Stanton numbers, and the friction factors in

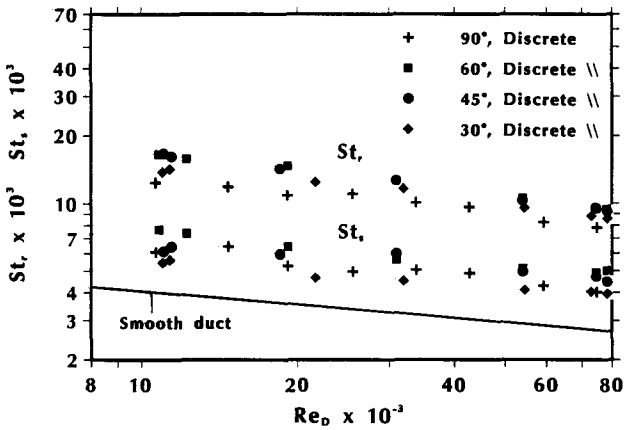

Fig. 5 Ribbed Wall and Smooth Wall Stanton Numbers as Functions of Reynolds Number, Parallel Discrete Rib Cases

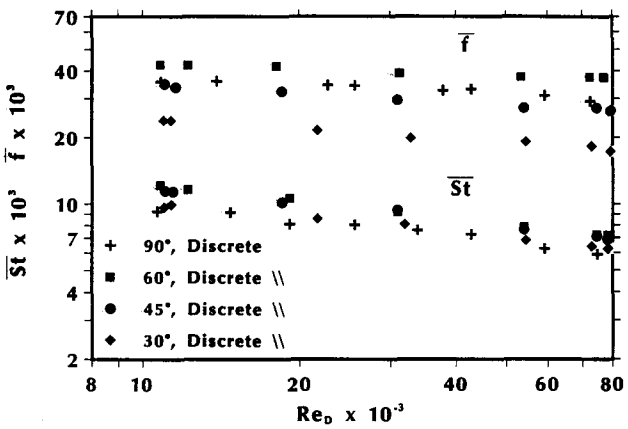

Fig. 6 Average Stanton Number and Friction Factor as Functions of Reynolds Number, Parallel Discrete Rib Cases

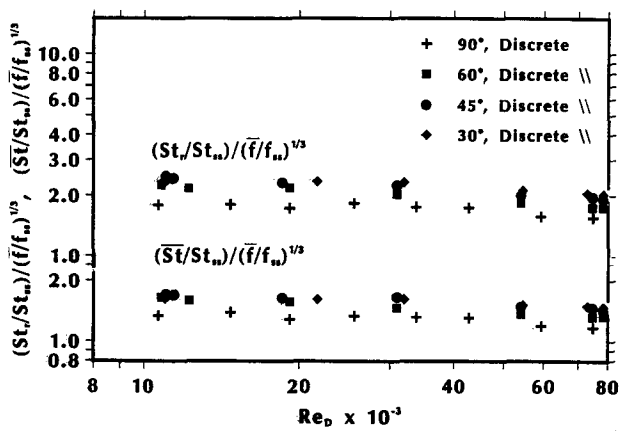

Fig. 7 Thermal Performances of Parallel Discrete Ribs, $[(St_r/St_{ss})/(\bar{f}/f_{ss})^{1/3}]$ and $[(\bar{St}/St_{ss})/(\bar{f}/f_{ss})^{1/3}]$ as Functions of Reynolds Number

the crossed angled discrete rib cases are all lower than those in the 90° discrete rib cases. The thermal performances of crossed angled discrete ribs are not as good as that of 90° discrete ribs.

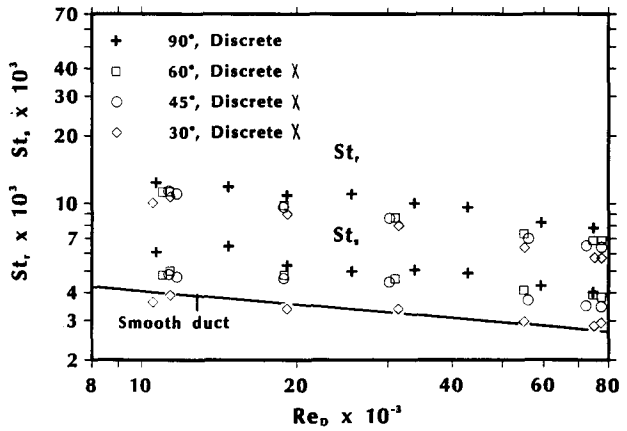

Fig. 8 Ribbed Wall and Smooth Wall Stanton Numbers as Functions of Reynolds Number, Crossed Discrete Rib Cases

Based on the values of the ratios $[(St_r/St_{ss})/(\bar{f}/f_{ss})^{1/3}]$ and $[(\bar{St}/St_{ss})/(\bar{f}/f_{ss})^{1/3}]$ in the various parallel and crossed angled rib cases studied, parallel angled ribs (including both full and discrete ribs) perform consistently better than corresponding crossed angled ribs. Metzger and Vendula (1987), Han and Zhang (1989), Han et al. (1989), and Lau et al. (1989) all drew similar conclusions. The good thermal performances in the parallel angled rib cases may have been the results of the mixing of the main flow with the counter-rotating vortices in the two opposite halves of the channel caused by secondary flow near the parallel rib arrays on the two opposite walls.

Comparisons of Full and Discrete Rib Arrays

In Figs. 11, 12, and 13, the ribbed wall heat transfer, the smooth wall heat transfer, the overall heat transfer, the overall pressure drops, and the thermal performances in the parallel angled discrete rib cases are compared to their counterparts in corresponding parallel angled full rib cases. The ribbed wall heat transfer in the parallel 60° and 45° discrete rib cases is about 5 to 11 percent higher than that in the parallel 60° full rib case and is about 14 to 31 percent higher than that in the 45° full rib case, over the range of Reynolds number studied (see

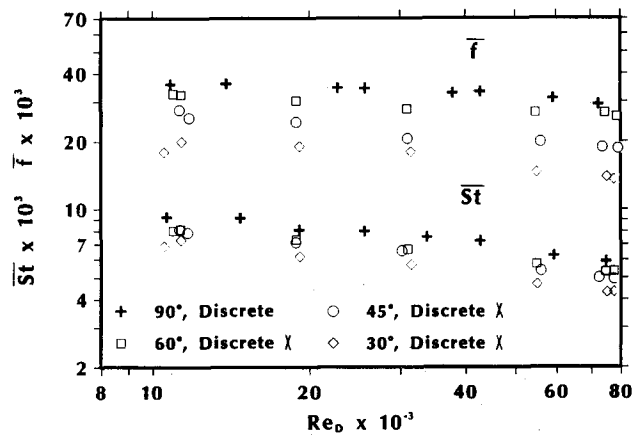

Fig. 9 Average Stanton Number and Friction Factor as Functions of Reynolds Number, Crossed Discrete Rib Cases

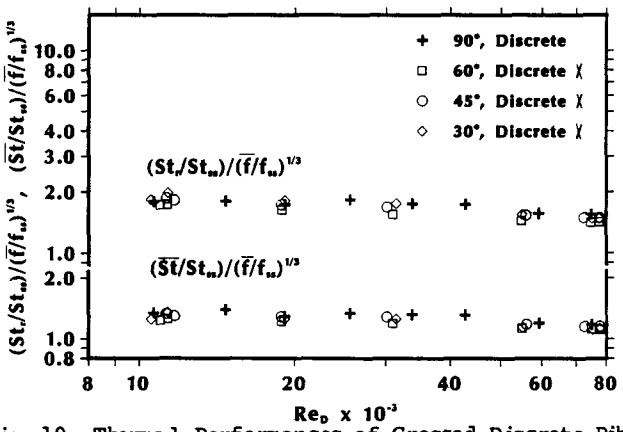

Fig. 10 Thermal Performances of Crossed Discrete Ribs, $[(St_r/St_{ss})/(\bar{f}/f_{ss})^{1/3}]$ and $[(\bar{St}/St_{ss})/(\bar{f}/f_{ss})^{1/3}]$ as Functions of Reynolds Number

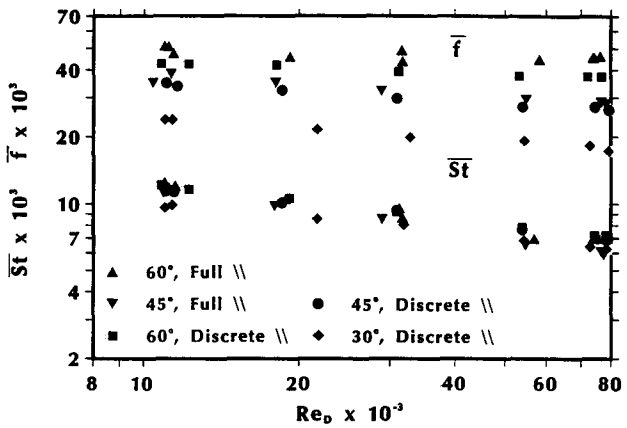

Fig. 12 Comparisons of Average Stanton Numbers and Friction Factors in Parallel Angled Rib Cases

Fig. 11). The smooth wall heat transfer in the parallel angled discrete rib cases, however, is lower that in the parallel angled full rib cases.

Included in Fig. 11 for comparison are the parallel 60°, 45°, and 30° discrete rib results from Lau et al. (1989). The ribbed wall Stanton numbers in the parallel angled discrete rib cases in this study are always as high as or slightly higher than those in corresponding discrete rib cases in the earlier study.

Figure 12 shows that 60° and 45° discrete ribs enhance the overall heat transfer to the cooling air slightly more than 60° and 45° full ribs and cause lower pressure drops than 60° and 45° full ribs. As a result, the values of $[(St_r/St_{ss})/(\bar{f}/f_{ss})^{1/3}]$ and $[(\bar{St}/St_{ss})/(\bar{f}/f_{ss})^{1/3}]$ in the 60° and 45° discrete rib cases are always higher than those in the 60° and 45° full rib cases (see Fig. 13). For a given pumping power, 60° discrete ribs enhance the ribbed wall heat transfer about 5 to 19 percent more than 60° full ribs, and 45° discrete ribs enhance the ribbed wall heat transfer about 11 to 32 percent more than 45° full ribs, over the range of Reynolds number studied. Because of the much lower values of $\bar{f}$, the values of $[(St_r/St_{ss})/(\bar{f}/f_{ss})^{1/3}]$ and $[(\bar{St}/St_{ss})/(\bar{f}/f_{ss})^{1/3}]$ in the 30° angled discrete rib case are as high as or higher than those in the 45° angled discrete case.

Parallel angled discrete ribs are superior to parallel angled full ribs and are recommended for internal cooling passages in gas turbine airfoils.

Parallel 30° discrete ribs have the highest thermal performance but their performance is only slightly better than that of parallel 45° discrete ribs. Han et al. (1985) and Han and Park (1988) observed the same trend for angled full ribs.

The roughness functions, $R(e^+)$, $G(e^+, Pr)$, and $\bar{G}(e^+, Pr)$, are expressed as power functions of the roughness Reynolds number, e^+. Figures 14 and 15 present the roughness functions in the various parallel angled rib cases. Parallel angled discrete ribs have lower values of $G(e^+, Pr)$ and $\bar{G}(e^+, Pr)$ than parallel angled full ribs since parallel angled discrete ribs cause higher heat transfer and lower pressure drop than corresponding full ribs.

Table 2 gives the coefficients and exponents in these functions for all cases studied. With Table 2 and equations 5 through 8, the Stanton numbers and friction factor can be predicted for given values of α, e/D and Re_D.

With Table 2 and the roughness function correlations given in Lau et al. (1989), the values of $G(e^+, Pr)$ and $\bar{G}(e^+, Pr)$ in the parallel 45° and 30° discrete rib cases in this study (with oblique arrays of segments of the 45° and 30° full ribs) are found to be consistently lower (up to 20 percent lower) than those in the parallel 45° and 30° discrete rib cases in Lau et al. (1989) (with arrays of segments of the 90° full ribs turned 45° and 30° with respect to the main flow), for $100 < e^+ < 1{,}000$. The corresponding values of $G(e^+, Pr)$ and $\bar{G}(e^+, Pr)$ in the two parallel 60°

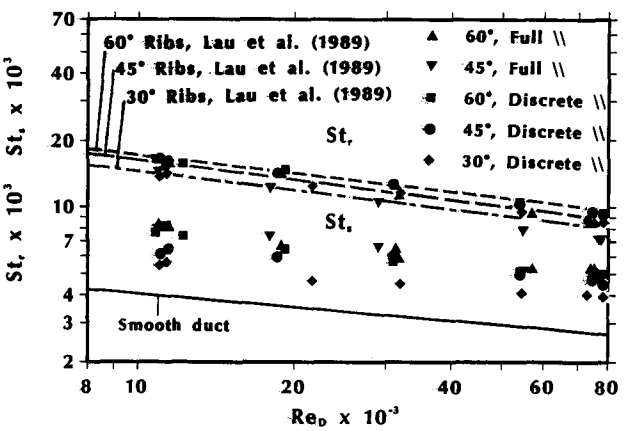

Fig. 11 Comparisons of Ribbed Wall and Smooth Wall Stanton Numbers in Parallel Angled Rib Cases

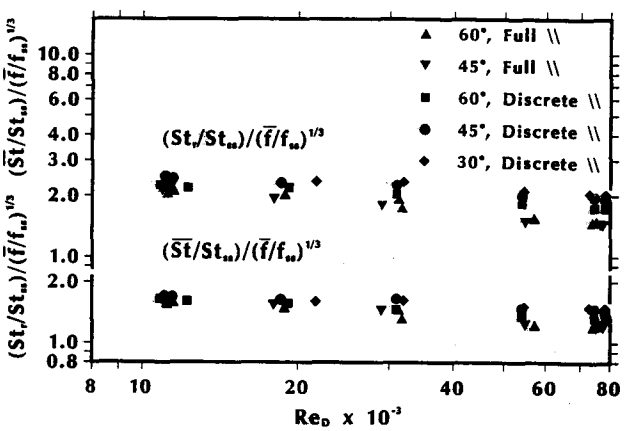

Fig. 13 Comparison of Thermal Performances of Parallel Angled Ribs

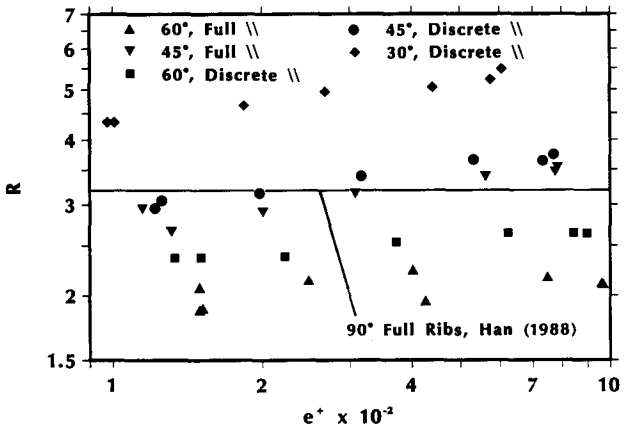

Fig. 14 $R(e^+)$ as a Function of e^+, Parallel Angled Rib Cases

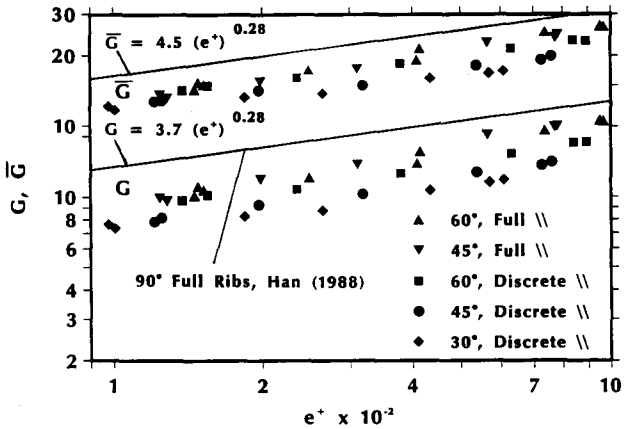

Fig. 15 $G(Pr, e^+)$ and $\bar{G}(Pr, e^+)$ as Functions of e^+, Parallel Angled Rib Cases

discrete rib cases in the two studies, however, are within ±5 percent of each other. Thus, the parallel 45° and 30° discrete rib arrays in this study have higher thermal performances than the parallel 45° and 30° discrete rib arrays in Lau et al. (1989).

CONCLUDING REMARKS

Based on the results of this investigation, the following conclusions can be drawn:

(1) Parallel angled discrete ribs are superior to parallel angled full ribs and are recommended for internal cooling passages in gas turbine airfoils. For a given pumping power, 60° and 45° discrete ribs enhance the ribbed wall heat transfer about 5 to 19 percent and about 11 to 32 percent more than the corresponding angled full ribs, over the range of Reynolds number studied. Parallel 30° discrete ribs have the highest thermal performance but their performance is only slightly better than that of parallel 45° discrete ribs.

(2) For $\alpha = 60°$ and 45°, parallel discrete ribs have higher ribbed wall heat transfer, lower smooth wall heat transfer, and lower channel pressure drop than parallel full ribs. The ribbed wall heat transfer in the parallel 60° and 45° discrete rib cases is about 5 to 11 percent higher than that in the parallel 60° full rib case and is about 14 to 31 percent higher than that in the 45° full rib case, over the range of Reynolds number studied.

(3) Parallel 60° discrete ribs have the highest ribbed wall heat transfer and parallel 30° discrete ribs cause the lowest pressure drop.

(4) The parallel 45° and 30° discrete ribs in this study have higher thermal performances than the parallel 45° and 30° discrete ribs in Lau et al. (1989).

(5) The Stanton numbers and the friction factors in the crossed angled full and discrete rib cases are all lower than those in the corresponding 90° and parallel angled rib cases. Crossed angled ribs have poor thermal performance and are not recommended.

TABLE 2 Coefficients and Exponents for the Functions $R(e^+)$, $G(e^+, Pr)$, and $\bar{G}(e^+, Pr)$

Case	$R(e^+)=a(e^+)^b$		$G(e^+,Pr)=a(e^+)^b$		$\bar{G}(e^+,Pr)=a(e^+)^b$	
	a	b	a	b	a	b
1	2.269	0.055	3.728	0.267	5.447	0.250
2a	1.641	0.038	1.488	0.387	2.855	0.328
2b	2.395	0.078	2.514	0.340	5.096	0.260
3a	1.556	0.122	1.428	0.398	2.627	0.335
3b	1.854	0.172	3.181	0.303	4.348	0.280
4	1.848	0.086	3.884	0.229	5.894	0.214
5a	1.710	0.065	2.074	0.309	3.802	0.267
5b	2.114	0.089	3.473	0.265	6.902	0.202
6a	1.698	0.119	1.797	0.309	3.981	0.239
6b	1.913	0.154	3.049	0.269	6.080	0.207
7a	2.557	0.115	2.288	0.252	4.642	0.202
7b	3.044	0.121	2.330	0.305	5.429	0.223

ACKNOWLEDGEMENTS

This research was supported in part by the National Science Foundation (Grant No. CBT-8713833).

REFERENCES

Burggraf, F., 1970, "Experimental Heat Transfer and Pressure Drop with Two-Dimensional Turbulence Promoter Applied to Two Opposite Walls of a Square Tube," in Augmentation of Convective Heat and Mass Transfer, edited by Bergles, A.E. and Webb, R.L., ASME, New York, pp. 70-79.

Han, J.C., 1984, "Heat Transfer and Friction in

Channels with Two Opposite Rib-Roughened Walls," ASME Journal of Heat Transfer, Vol. 106, pp. 774-781.

Han, J.C., 1988, "Heat Transfer and Friction Characteristics in Rectangular Channels with Rib Turbulators," ASME Journal of Heat Transfer, Vol. 110, pp. 321-328.

Han, J.C., Ou, S., Park, J.S., and Lei, C.K., 1989, "Augmented Heat Transfer in Rectangular Channels with Narrow Aspect Ratios with Rib Turbulators," Int. J. of Heat and Mass Transfer, in press.

Han, J.C. and Park, J.S., 1988, "Developing Heat Transfer in Rectangular Channels with Rib Turbulators," Int. J. of Heat and Mass Transfer, Vol. 31, pp. 183-195.

Han, J.C., Park, J.S., and Lei, C.K., 1985, "Heat Transfer Enhancement in Channels with Turbulence Promoters," ASME Journal of Engineering for Gas Turbines and Power, Vol. 107, pp. 629-635.

Han, J.C. and Zhang, P., 1989, "Effect of Rib-Angle Orientation on Local Mass Transfer Distribution in a Three-Pass Rib-Roughened Channel," ASME Paper No. 89-GT-98.

Kline, S.J. and McClintock, F.A., 1953, "Describing Uncertainties in Single-Sample Experiments," Mechanical Engineering, Vol. 75, pp. 3-8.

Lau, S.C., McMillin, R.D., and Han, J.C., 1989, "Turbulent Heat Transfer and Friction in a Square Channel with Discrete Rib Turbulators," accepted for presentation at ASME Winter Annual Meeting, San Franscisco, CA, and for publication in ASME Journal of Turbomachinery.

Metzger, D.E. and Vendula, R.P., 1987, "Heat Transfer in Triangular Channels with Angled Roughness Ribs on Two Walls," Experimental Heat Transfer, Vol. 1, pp. 31-44.